Proceedings of the 2003 IEEE
International Conference on Robotics & Automation
Taipei, Taiwan, September 14-19, 2003

Dynamic Modeling of the Body Inversion for Automated Transfer of Live Birds

Kok-Meng Lee and Chris Shumway
The George W. Woodruff School of Mechanical Engineering
Georgia Institute of Technology
Atlanta, Georgia 30332-0405
Correspondence email: kokmeng.lee@me.gatech.edu

ABSTRACT:- Body rotation under free fall along a desired trajectory can be found in many applications such as sports, entertainment, and manufacturing. An appropriately designed body path could lower the forces at the joints during inversion and thus minimizing potential injury. This paper presents a method of developing dynamic models that characterize the interaction between the body of a live object undergoing inversion and the mechanical system driving the rotation. The method offers an effective means to analyze the sensitivity of the design and operational parameters on the body rotation. The models have been validated experimentally. The simulated and experimental results offer significant insights to the joint forces and a means to improve the body dynamics. While the results have immediate application in inverting live birds for poultry meat processing, we expect the model will provide a basis for analyzing body rotational dynamics in other applications such as gymnastics and roller coasters.

Index terms: body rotation, live-bird handling automation, inversion, prototyping, design simulation

1. INTRODUCTION

Body rotation can be found in many applications such as sports, inversion therapy, entertainment, and manufacturing. An appropriate designed body path could lower the forces at the joints during inversion and thus minimize potential injuries. A good understanding of the interaction between the body undergoing inversion and the mechanical system driving the rotation can offer significant insights to the influences of the design parameters, the gravity, the initial momentum, and the external forces on the body trajectory and the joint forces.

Body rotation has been studied in many different fields. In the pole-vault event in track and field [Hubbard, 1980; Griner 1984], the design of the highly elastic pole must take into account the body rotation of the vaulter who applies a compressive load and a bending moment to the upper end of the pole during the vault. In therapy, the inversion of the human body has been used to relieve back and neck pain by gently stretching the vertebrae using the person's own body weight. In manufacturing of meat products, objects must be inverted for subsequent processing. In robotics, the nature of a gymnastic maneuver was originally examined for the purpose of programming a mechanism to execute a forward flip [Hodgins and Raibert, 1990] or computer graphic animation [Raibert *et al.*, 1993]. Saito and Fukuda [1994] studied the motion of a long-arm ape for designing Brachiation robots, much like a gymnast on a high bar. These early researches were motivated by the design and control of mobile robots, the dynamic models were generally based on relatively simple mechanisms. More recently, dynamic models were developed to help coaches teach novice gymnasts the kip [Nakawaki *et al.*, 1998], develop more sophisticated skilful motion on a high bar [Michitsuji *et al.* 2001], or better understand the skill required to perform backward giant circling on the rings [Yamada *et al.* 2002]. These investigations formulated the gymnast as a three-link pendulum system, focusing on the body rotation about a specific, stationary point under the influences of gravity.

Unlike most of published works in robotics, where the emphasis has been placed on the control of a mechanism aimed at animating a live subject, this paper focuses on developing models and algorithms to characterize the body dynamics under the influences of the mechanical system that drives the body inversion. The equations of body rotational motion are derived using the Lagrangian method, which are subject to constraints imposed by the track on which the body is transported and the motion limit of the limbs. Although a number of methods have been proposed for analyzing complex mechanisms, for example [Chen, 1998; Caputo 2001], no experimental verification was attempted in these publications. This paper offers the following:

(1) The formulation of an inversion system, which takes into account the dynamics of both the body undergoing inversion and the mechanical system driving the rotation, is presented:

Using a set of well-defined system parameters and a set of redundant generalized coordinates, we offer an effective method to analyze the sensitivity of the system/body parameters on the dynamic loading of the driving mechanism as well as the resulting forces/torques at the joints of the rotating body.

(2) The model has been experimentally validated:

The dynamic models have been validated by comparing the simulations against results obtained experimentally. The error is estimated by calculating the residuals of the constraint equations, which should equal to zero if the constraints are satisfied. The maximum error was found within 0.3mm.

(3) A simulation algorithm for assessing the effects of the design changes has been demonstrated:

The validated model has an immediate application in automating live-bird inversion process for poultry meat process, which has been used to analyze the effects of inversion track design on the joint forces and improve the body dynamics during rotation.

It is expected that the models presented here will provide a basis for analyzing body rotational dynamics in other applications such as gymnastics and roller coasters.

2. SYSTEM OVERVIEW

Figure 1 shows the inverter which consists of the chain-conveyor and the trolley on which the pallet is mounted. The trolley is controlled by a motor-gear-chain mechanism via a link connecting the chain and the trolley by means of pin joints at P_g and A_1. The reference coordinate system XY is attached at the

driving shaft as shown in Figure 1. The rollers, P_f and P_b, follow the pre-defined elliptical inversion path:

$$\frac{X^2}{e_X^2}+\frac{Y^2}{e_Y^2}=1$$

where e_X and e_Y are the characteristic dimensions of the inversion path along the X and Y-axes respectively. The pallet is constrained to move perpendicularly to the trolley through a spring-damper system. The trolley can be characterized by the following parameter vector:

$$D=\begin{bmatrix} e_X & e_Y & r_g & d_1 & d_2 & d_3 & h_o & \varepsilon \end{bmatrix}^T$$

where d_1 is the length of the connecting link; d_2 and d_3 are the distances of the front and back rollers from A_1 respectively; h_o is the nominal length of the spring-damper system; r_g is the gear radius; and ε is the distance between J_1 and A_3. For a given chain velocity v_g, the pallet has only one DOF (the displacement of A_3 with respect to A_2 from its nominal position.

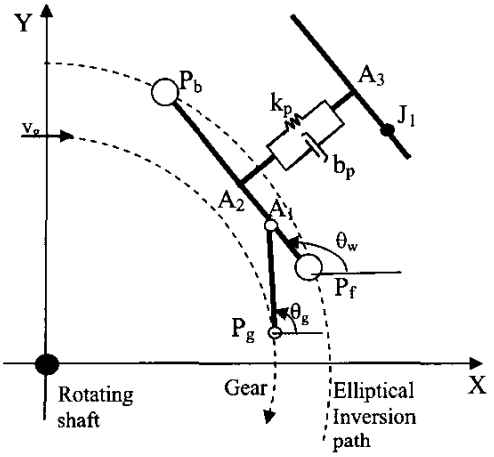

Figure 1 Schematics of the gear-chain-trolley mechanism

The object is modeled as a 2D, 4-limb serial mechanism as shown in Figure 2, where J_1, J_2, J_3, J_4 and J_c are the foot, ankle, knee, hip joints and the body center respectively. The variation of the object sizes can be characterized by the vector S:

$$S=\begin{bmatrix} \ell_1 & \ell_2 & \ell_3 & \ell_4 & \varphi & \eta & \lambda & m \end{bmatrix}^T$$

where ℓ_1, ℓ_2, and ℓ_3 represents the lengths of the foot, shank, and thigh respectively; ℓ_4 denotes the distance between J_4 and J_c; φ is the angle between ℓ_4 and the x-axis as shown in Figure 2; η and λ represent the characteristic dimensions of the body (or link 4); and m is the mass of the body. The 2D mechanism has 3-DOF (X_c, Y_c, φ_c) but 4 degrees of mobility (φ_1, φ_2, φ_3, φ_4) and thus, it has one kinematical redundancy. However, since J_1 is fixed on the pallet surface and φ_2 and φ_3 rotate between 0° and 180°, the motions of J_2 and J_3 have finite ranges.

3. ANALYTICAL MODEL

The model of the body inversion is formulated using Lagrange dynamics. The generalized coordinates characterizing the motion are defined by the vector

$$q=\begin{bmatrix} q_p & q_b \end{bmatrix}^T$$

where $q_p=\begin{bmatrix} P_{gX} & P_{gY} & P_{fX} & P_{fY} & P_{bX} & P_{bY} & \theta_g & \theta_w & h \end{bmatrix}^T$

$$q_b=\begin{bmatrix} J_{1X} & J_{1Y} & \varphi_1 & \varphi_2 & \varphi_3 & \varphi_4 & X_c & Y_c & \varphi_c \end{bmatrix}^T,$$

and X_c and Y_c are the position coordinates of J_c. Since the pallet has 1-DOF and the object has 3-DOF with one kinematical redundancy, the system is subject to 13 constraints given by Equations (1)-(10), which relate the 18 generalized coordinates.

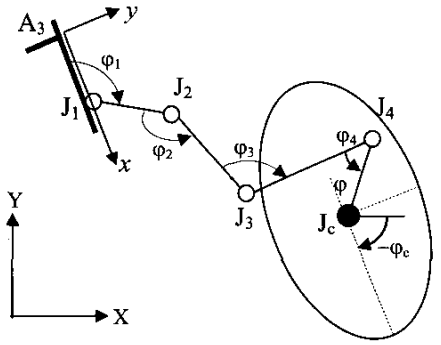

Figure 2: Schematic illustrating the object kinematics

3.1 Kinematical Constraints

For a specified angular rotation θ_r, the position and orientation of the object can be described by Equations (1) and (2) respectively:

$$\begin{bmatrix} X_c \\ Y_c \end{bmatrix}=\underline{J}_1+\ell_1\begin{bmatrix} \cos\phi_1 \\ \sin\phi_1 \end{bmatrix}-\ell_2\begin{bmatrix} \cos\phi_2 \\ \sin\phi_2 \end{bmatrix}+\ell_3\begin{bmatrix} \cos\phi_3 \\ \sin\phi_3 \end{bmatrix}-\ell_4\begin{bmatrix} \cos(\varphi_5-\varphi_c) \\ \sin(\varphi_5-\varphi_c) \end{bmatrix} \quad (1)$$

$$\varphi_c=\phi_4+\theta_w-\pi+\varphi \quad (2)$$

where

$$\begin{bmatrix} J_{1X} \\ J_{1Y} \end{bmatrix}=\underline{P}_g+d_1\begin{bmatrix} \cos\theta_g \\ \sin\theta_g \end{bmatrix}+\left(\frac{d_3-d_2}{2}-\varepsilon\right)\begin{bmatrix} \cos\theta_w \\ \sin\theta_w \end{bmatrix}+(h_0+h)\begin{bmatrix} \sin\theta_w \\ -\cos\theta_w \end{bmatrix} \quad (3)$$

$$\begin{bmatrix} P_{gX} \\ P_{gY} \end{bmatrix}=\begin{bmatrix} r_g\cos\theta_r \\ r_g\sin\theta_r \end{bmatrix} \quad (4)$$

and $$\phi_n=\theta_w+\sum_{m=1}^{n}(-1)^m\varphi_m$$

Since the trolley is constrained to follow the inversion path, the roller positions, (P_{fX}, P_{fY}) and (P_{bX}, P_{bY}), must be solved from the following set of non-linear constraint equations in order to determine the angular displacements θ_g and θ_w:

$$\frac{P_{fX}^2}{e_X^2}+\frac{P_{fY}^2}{e_Y^2}=1 \quad (5)$$

$$\frac{P_{bX}^2}{e_X^2}+\frac{P_{bY}^2}{e_Y^2}=1 \quad (6)$$

$$\left(P_{bX}-P_{fX}\right)^2+\left(P_{bY}-P_{fY}\right)^2=\left(d_2+d_3\right)^2 \quad (7)$$

$$\left(P_{fX}+d_2\cos\theta_w-P_{gX}\right)^2+\left(P_{gX}+d_2\sin\theta_w-P_{gY}\right)^2=d_1^2 \quad (8)$$

Once the locations of the rollers are known with respect to the XY frame, the angular displacements, θ_g and θ_w, can be determined from Equations (9) and (10):

$$\theta_g=\tan^{-1}\left(\frac{P_{fY}+d_2\sin\theta_w-P_{gY}}{P_{fX}+d_2\cos\theta_w-P_{gX}}\right) \quad (9)$$

$$\theta_w = \tan^{-1}\left(\frac{P_{bY} - P_{fY}}{P_{bX} - P_{fX}}\right) \tag{10}$$

3.2 Additional Constraints at Contact Area

Figure 3 illustrates the forces at the contact area between the object and the pallet, where f_n, and f_t are the normal and tangential components of the reaction acting on the object, and τ is the corresponding moment about the object center. Based on the conditions at the contact area, the inversion process can be divided into three regions.

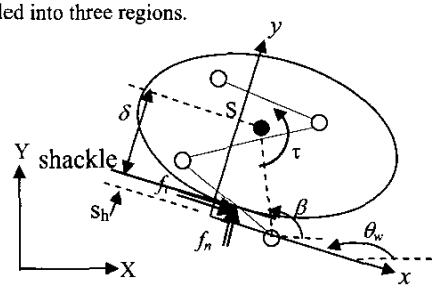

3(a) Forces and moment at the contact

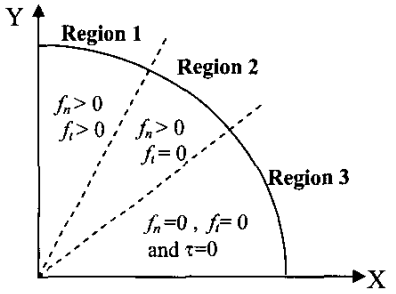

3(b) Conditions for transition

Figure 3 Constraints imposed at contact area

Region 1:

The body is in contact with the surface and is prevented to move backward (which could arise when the mechanical system starts from rest). Thus, $f_n > 0$ and $f_t > 0$, and the bird center is fixed with respect to the toe joint J_1.

$$\ell_T \sin(\theta_w - \beta) = s_h + \delta \tag{11}$$

where $$\ell_T = \sqrt{(J_{cX} - J_{1X})^2 + (J_{cY} - J_{1Y})^2}$$

$$\beta = \tan^{-1}\left(\frac{J_{cY} - J_{1Y}}{J_{cX} - J_{1X}}\right)$$

and $$\Delta^2 = (J_{cX} - S_X)^2 + (J_{cY} - S_Y)^2 \tag{12}$$

where $$\begin{bmatrix} S_X \\ S_Y \end{bmatrix} = \underline{F}_w + d_2 \begin{bmatrix} \cos(\theta_w) \\ \sin(\theta_w) \end{bmatrix} + (h + s_h + \lambda) \begin{bmatrix} \sin(\theta_w) \\ -\cos(\theta_w) \end{bmatrix}$$

The underside of the object flattens which allows sliding but not rolling, causing the object orientation to remain parallel to the shackle surface.

$$\varphi_c = \theta_w - \pi \tag{13}$$

Region 2:

When the body slides forward but it remains in contact with the surface, $f_t = 0$ and $f_n > 0$. Equation (12) no longer applies.

Region 3:

The object body is no longer in contact with the surface. Equations (11)-(13) are removed since $f_n = 0$ and $f_t = 0$.

3.3 Dynamic Model

The time derivates of Equations (1) through (13) can be written in the following form:

$$[a]\underline{\ddot{q}} = \underline{0} \tag{14}$$

where $[a]$ is a nxN Jacobian matrix for N generalized coordinates and n constraint equations. The Lagrange equations of motion can be written as

$$\frac{d}{dt}\left(\frac{\partial T(\dot{q}, q)}{\partial \dot{q}_j}\right) - \frac{\partial T(\dot{q}, q)}{\partial q_j} + \frac{\partial D(\dot{q})}{\partial \dot{q}_j} + \frac{\partial U(q)}{\partial q_j} = Q_j + \sum_{i=1}^{n} \lambda_i a_{ij}(q) \tag{15}$$

where the kinetic energy

$$T(\dot{q}, q) = \frac{1}{2}\sum_{i=1}^{7}(m_i V_i^2 + I_i \omega_i^2)\,; \tag{16}$$

the Rayleigh dissipation function

$$D(\dot{q}) = \frac{1}{2} b_P y^2 + \frac{1}{2}\sum_{i=1}^{4} b_i \varphi_i^2\,; \tag{17}$$

the potential energy

$$U(q) = \sum_{i=1}^{7} m_i g P_{iY} + \frac{1}{2} k_P y^2 + \frac{1}{2}\sum_{i=1}^{4} k_i \delta_i^2\,; \tag{18}$$

Q_j is the external forces applied on the system; and the last term accounts for the constraints through the Lagrange multiplier λ_i. In Equations (16) and (18), m_i and I_i (I = 1, ..., 7) are the masses and the moments of inertia of the connecting link, the trolley, the pallet, the four limbs of the bird respectively; P_{iY} and V_i are the Y-component position and the absolute velocity at the center of the i^{th} mass; and ω_i is the component of the vector defined by

$$\underline{\omega} = \begin{bmatrix} \dot{\theta}_G & \dot{\theta}_w & \dot{\theta}_w & \dot{\phi}_1 & \dot{\phi}_2 & \dot{\phi}_3 & \dot{\phi}_4 \end{bmatrix}^T \tag{19}$$

Due to the space limitation, the detailed derivation is omitted, which can be shown that Equations (15) has the form:

$$[M(q)]\ddot{q} + [C(\dot{q}, q)]\dot{q} + D_V(\dot{q}) + G(q) = Q + [a(q)]^T \lambda \tag{20}$$

where $$[M(q)] = \left[\frac{\partial^2 T(\dot{q}, q)}{\partial \dot{q}_1^2} \cdots \frac{\partial^2 T(\dot{q}, q)}{\partial \dot{q}_j^{\,2}} \cdots \frac{\partial^2 T(\dot{q}, q)}{\partial \dot{q}_n^2}\right]^T \tag{21}$$

$$[C(\dot{q}, q)]\dot{q} = \left[\cdots\left(\frac{\partial^2 T(\dot{q}, q)}{\partial q_j \partial \dot{q}_j}\dot{q} - \frac{\partial T(\dot{q}, q)}{\partial q_j}\right)\cdots\right]^T \tag{22}$$

$$D_V(\dot{q}) = \frac{\partial D(\dot{q})}{\partial \dot{q}_j} \tag{23}$$

$$G(q) = \frac{\partial U(q)}{\partial q_j} \tag{24}$$

$$[a(q)]^T \lambda = \sum_{i=1}^{n} \lambda_i a(q)_{i,j} \tag{25}$$

Equation (20) is in derivative form while its constraint equations are algebraic. In order to convert the coupled differential-algebraic equation into a form more appropriate for

computation, the time derivative of the velocity constraint Equation (14) is used:

$$[a]\ddot{q} + [\dot{a}]\dot{q} = \underline{0} \tag{26}$$

Equations (20) and (26) are augmented, which result in the following form:

$$\begin{bmatrix} [M(q)] & -[a]^T \\ -[a] & [0] \end{bmatrix} \begin{Bmatrix} \ddot{q} \\ \lambda \end{Bmatrix} = \begin{Bmatrix} Q - [F(q,\dot{q})]\dot{q} \\ [\dot{a}]\dot{q} \end{Bmatrix} \tag{27}$$

where $F(\dot{q},q) = [C(\dot{q},q)]\dot{q} + D_V(\dot{q}) + G(q)$.

At any time instant, the numerical values for the generalized position vector $\underline{q}$ and velocity vector, $\dot{\underline{q}}$, are known; thus, the numerical values of $[M(\underline{q})]$, $\underline{F}(\dot{\underline{q}},\underline{q})$, $[a(\underline{q})]$, and $[\dot{a}(\underline{q})]$ can be computed. To explicitly solve $\ddot{\underline{q}}$ and $\underline{\lambda}$, Equation (27) is rewritten as

$$\begin{Bmatrix} \ddot{\underline{q}} \\ \underline{\lambda} \end{Bmatrix} = \begin{bmatrix} [M(\underline{q})] & -[a(\underline{q})]^T \\ -[a(\underline{q})] & [0] \end{bmatrix}^{-1} \begin{Bmatrix} Q - \underline{F}(\dot{q},q) \\ [\dot{a}(\underline{q})]\dot{\underline{q}} \end{Bmatrix} \tag{28}$$

With appropriate initial conditions, the above equation can be solved numerically. The forces/torques acting at the toe, ankle, knee and hip joints corresponding to $\varphi_1, \varphi_2, \varphi_3$, and φ_4 respectively can then be calculated from $[a(q)]^T \lambda$:

$$\tau_1 = \lambda_1 \sum_{i=1}^{3} \ell_i s_i (-1)^{i-1} - \lambda_2 \sum_{i=1}^{3} \ell_i c_i (-1)^{i-1} - \lambda_3 \tag{30a}$$

$$\tau_2 = \lambda_1 \sum_{i=2}^{3} \ell_i s_i (-1)^{i} - \lambda_2 \sum_{i=2}^{3} \ell_i c_i (-1)^{i} + \lambda_3 \tag{30b}$$

$$\tau_3 = \ell_3 s_3 \lambda_1 - \ell_3 c_3 \lambda_2 - \lambda_3 \tag{30c}$$

$$\tau_4 = \lambda_3 \tag{30d}$$

where λ_1, λ_2 and λ_3 are the Lagrange multipliers associated with the velocity constraints derived from the X and Y components of Equation (1) and (2) respectively.

4. SIMULATION RESULTS

Since the model has an immediate application in live bird handling [Lee, 2000], the object chosen is a model bird mechanism designed with dimensions from a typical broiler so that the dynamic models presented above can be experimentally verified before testing with a live bird. Simulations were performed based on the design of a live-bird inverting system developed at Georgia Tech as shown in Figure 4. The values of the design and object parameters used in the simulation are given as follows:

$$D = [111 \quad 148 \quad 147 \quad 100 \quad 65 \quad 65 \quad 140 \quad 30]^T$$

$$S = [70 \quad 90 \quad 80 \quad 60 \quad 37 \quad 57 \quad 97 \quad 1.6]^T$$

where lengths are in mm; angles in degrees; and mass in kilograms (kg). The masses for the connecting rod, the trolley and the pallet are 0.1, 1.1, and 3.4 kg respectively. The masses for the limbs ℓ_1, ℓ_2 and ℓ_3 and ℓ_4 are 0.03, 0.08, and 0.1 kg. The masses are assumed at the mid points of the respective components (or the limbs). The mass of the body is 1.6 kg.

In the simulation, the non-conservative external force vector Q is assumed to be empty and s_h is 2.5mm. The coefficients for the spring and damper in the pallet suspension are 4.68kN/m and 11.1 Ns/m respectively. Before the inversion, the bird moves with the pallet at a chain speed of 0.457m/s, and the velocities in the Y direction are assumed to be zero. Other initial conditions are given as follows:

$$q_p(0) = [-20 \quad -147 \quad -57 \quad 148 \quad -184 \quad 148 \quad 180 \quad 180 \quad 126]^T$$

$$q_b(0) = [-90 \quad 273 \quad 5 \quad 40 \quad 58 \quad -14 \quad -108 \quad 333 \quad 0]^T$$

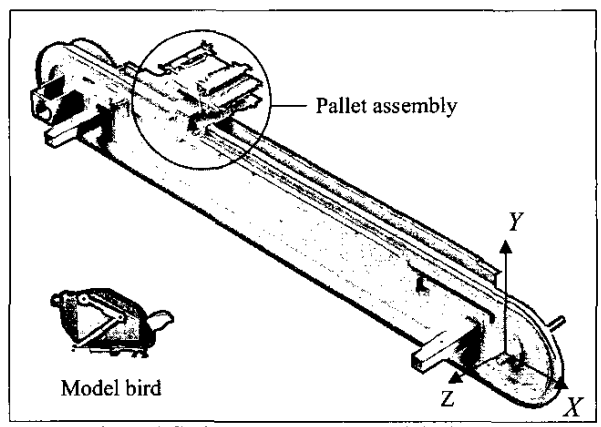

Figure 4 CAD model o the bird and the inverter

Figure 5 shows the trajectory of the body as it inverts, which the dashed lines divide the three regions as described in Figure 3(b). Still shot 1 is in Region #1 where $f_n > 0$ and $f_t > 0$. Still shot 2 is in Region #2 where the ellipse is sliding down the shackle but remains in contact with the shackle, where $f_n > 0$ and $f_t = 0$. Still shots 3 through 7 are in Region #3 where $f_n = f_t = 0$, where still shot 3 shows the bird body just leaving contact with the shackle surface, while still shot 7 shows the end of the simulation.

In the numerical computation, the transition from one region to the next is determined by the reaction forces acting on the bird by the mechanical system, f_n and f_t. Since only the algebraic sign of these constraint forces are needed the Lagrange multipliers associated with the velocity constraints derived from Equations (10) and (11) can be used to avoid the complexity of computing. Figure 6 is a plot showing the Lagrange multipliers that represent the constraint forces, f_n and f_t, and thus the progression from region to region.

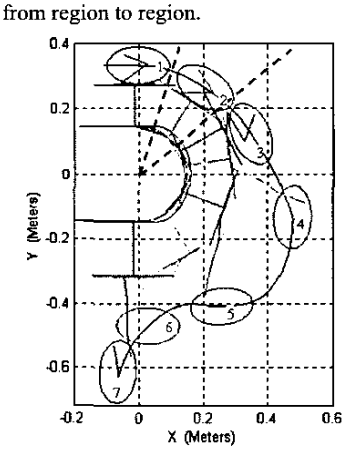

Figure 5 Simulated body trajectory

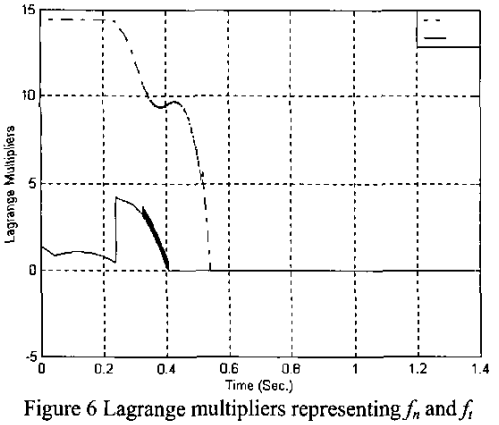

Figure 6 Lagrange multipliers representing f_n and f_t

Figure 7 shows the angular velocity of the orientation experiencing a sudden increase at t = 0.72second, which corresponds to the still shot 4 in Figure 5. The body approaches –90° and then rotates back to above horizontal (or 0°). This is undesired since once the body is inverted it should kept at the orientation φ_c=–90°. The velocity change, as seen in still shot 4, is contributed to the bird limb angles reaching their respective maximums. In other words, the limbs have been stretched out to a singularity configuration, and the bird body rotates about point J_4 as illustrated in Figure 8. To accomplish J_4 rotation, an internal force from the stretched limbs is applied onto the bird body, which also causes the angular velocity and thus the bird angular momentum to rapidly change.

The simulation error can be estimated by calculating the residuals of the constraint equations, which should equal to zero if the constraints are satisfied. Figure 9 graphs the constraints with the greatest errors, which is the constraint of the front wheel. The maximum value of the error is less than 0.3mm.

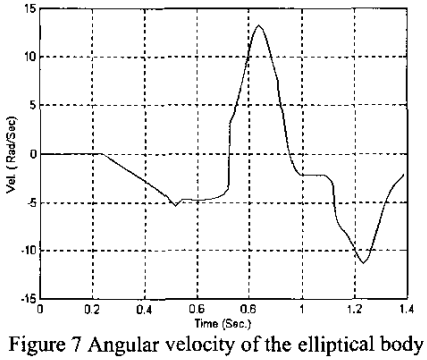

Figure 7 Angular velocity of the elliptical body

5. EXPERIMENTAL VERIFICATION

In order to validate the analytical model, an experiment was performed using the test bed developed at Georgia Tech. The two toe-joints J_1 of a model bird mechanism were fixed on the pallet by means of suction cups. The motion trajectory was recorded using a video camera and digitized for off-line analysis. Figure 10 shows the experimentally recorded trajectory of the model bird, which agrees well with the simulated centers. Similar comparison of the object orientation is graphed in Figure 11. These comparisons show the experimental results agree well with the trends predicted by simulation, where some discrepancies are expected since friction occurred in the physical joints were neglected in the model. At the instant when the bird body is at its singularity configuration which results in a drastic change in body orientation from –90° and then rotates back to approximately 0° as shown in Figures 12 (a) and (b) respectively.

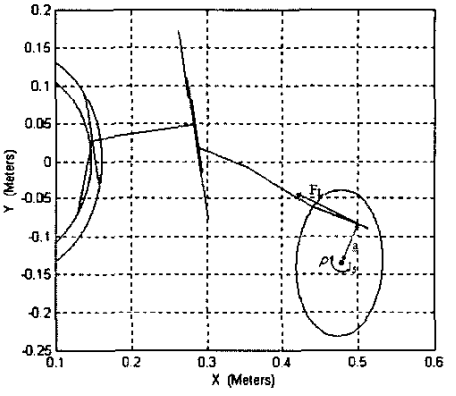

Figure 8 Configuration at the signularity

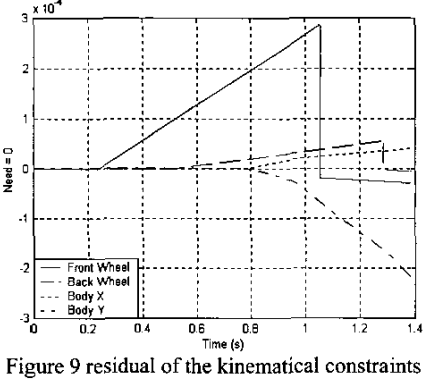

Figure 9 residual of the kinematical constraints

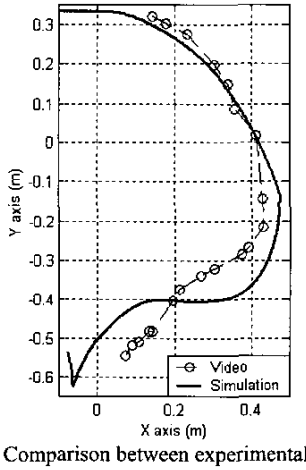

Figure 10 Comparison between experimental results and simulations of bird center

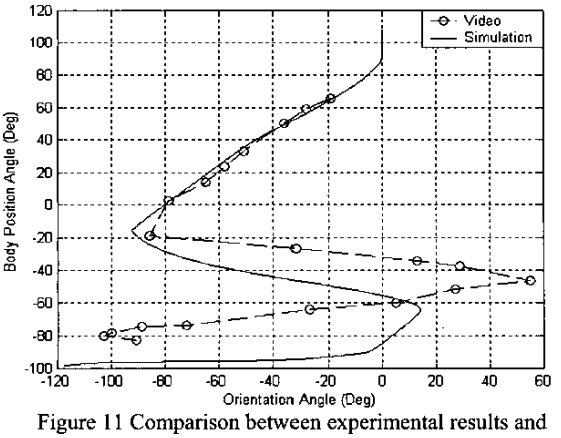

Figure 11 Comparison between experimental results and simulations of bird orientation

6. CONCLUSIONS

A dynamic model that characterizes the dynamics of the body undergoing inversion along a predetermined track has been developed. The model derived using constrained Lagrange dynamics offers an effective means to analyze the sensitivity of the design and operational parameters on the dynamics of the body and the forces and moments at the joints.

The model has been validated by comparing the simulated trajectory of the body against the results obtained experimentally. Comparisons show the experimental results agree well with the trends predicted by simulation.

Although the results presented here have an immediate application in meat processing industry, it is expected that the model will also provide a basis for analyzing body rotational dynamics in other applications such as sports, inversion therapy, entertainment, and manufacturing.

REFERENCE

Caputo, M.R., 2001, "Further Results on Lagrange Multipliers with Several Binding Constraints," Economic Letters 70, 335-340.

Chen, Y.H. 1998, Second-order Constraints for Equations of Motion of Constrained Systems, *IEEE/ASME Trans.on Mechatronics*, Vol 3. No. 3, September, 240-248.

Griner, G. M. 1984, "A Parametric Solution to the Elastic Pole Vaulting Pole Problem," *ASME Journal of Applied Mechanics*, Vol. 106.

Hodgins, J. K. and M. H. Raibert, 1990, "Biped Gymnastics," International Journal of Robotics Research, Vol. 9, No. 2 April, 115-132.

Habbard, M., "Dynamics of the Pole Vault," Journal of Biomechanics, Vol. 13, No. 11, 1980, 965-976.

Lee, K-M., 2000, "Design Criteria for Developing an Automated Live Bird Transfer System," *Proc. of the 2000 IEEE ICRA*, April 24-28, San Francisco, CA, Vol. 2, pp. 1138-1143; also in *IEEE Trans. on Robotics and Automation,* Vol. 17, Issue 4, Aug. 2001 pp. 483 -490.

Micitsuji, Y., H. Sato, and M. Yamakita, 2001, "Giant Swing via Forward Upward Circling of the Acrobat-Robot," *Proc. of ACC,* Arlington, VA, 3262-3267.

Nakawaki, D., S. Joo, and F. Miyazaki, 1998, "Dynamic Modeling Approach to Gymnastic Coaching," *Proc. of IEEE ICRA*, Leuven, Belgium 1069-1076.

Raibert, H. R., J. K. Hodgins, R.P. Playter, and R. P. Ringrose, 1993, "Animation of Legged Maneuvers: Jumps, Somersaults, and Gait Transitions," *JRSJ* Vol. 11, No.3, 333-342.

Saito, F., T. Fukuda, and F. Arai, 1994, "Swing and Locomotion Control for a Two-Link Brachiating Robot," *IEEE Control Systems,* February, 5-11.

Yamada, T., K. Watanabe, K. Kiguchi, and K. Izumi, 2002, "Acquiring Performance Skill of Backward Giant Circle by Rings Gymnastic Robot," *Proc. of IEEE ICRA*, Washington DC, 1565-1570.

ACKNOWLEDGEMENT

The Agriculture Technology Research Program (ATRP) and the U.S. Poultry and Eggs Association have supported this project. The test bed was developed with helps from the ATRP's staff.

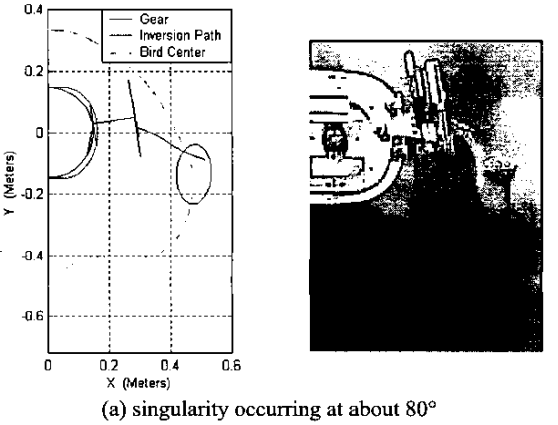

(a) singularity occurring at about 80°

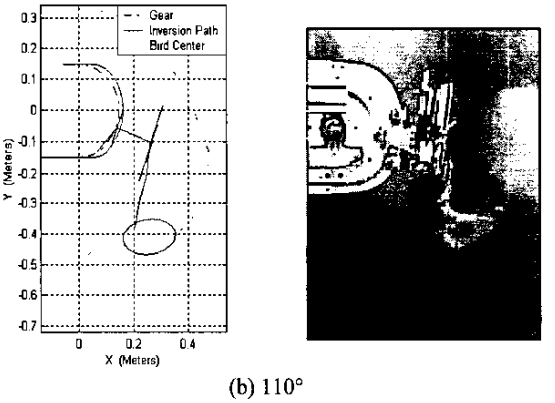

(b) 110°

Figure 12 Comparison between experimental results and simulations of bird configuration at singularity